



CHORUS

This is the accepted manuscript made available via CHORUS. The article has been published as:

Ab initio melting curve of osmium

L. Burakovsky, N. Burakovsky, and D. L. Preston

Phys. Rev. B **92**, 174105 — Published 9 November 2015

DOI: [10.1103/PhysRevB.92.174105](https://doi.org/10.1103/PhysRevB.92.174105)

Ab Initio Melting Curve of Osmium

L Burakovsky¹, N Burakovsky², and D L Preston²

¹ *Theoretical and* ² *Computational Physics Divisions,*

Los Alamos National Laboratory, Los Alamos, New Mexico 87545

Abstract

The melting curve of osmium up to a pressure (P) of 500 GPa is obtained from an extensive suite of *ab initio* quantum molecular dynamics (QMD) simulations using the Z method. The *ab initio* $P = 0$ melting point of Os is 3370 ± 75 K; this range encompasses all of the available data in the literature and corroborates the conclusion of Arblaster that the melting temperature of pure Os is 3400 ± 50 K and that the 3300 K typically quoted in the literature is the melting point of impure Os. The $T = 0$ equation of state (EOS) of Os and the P -dependence of the optimized c/a ratio for the hexagonal unit cell, both to pressures ~ 900 GPa, are obtained in the *ab initio* approach as validation of its use. Although excellent agreement with the available experimental data ($P \lesssim 80$ GPa) is found, it is the third-order Birch-Murnaghan EOS with $B'_0 = 5$ rather than the more widely accepted $B'_0 = 4$ that describes the QMD data to higher pressures, in agreement with the more recent experimental EOS by Godwal *et al.* The theoretical melting curve of Os obtained earlier by Joshi *et al.* is shown to be inconsistent with our QMD results, and the possible reason for this discrepancy is suggested. Regularities in the melting curves of Os and five other 3rd-row transition metals (Ta, W, Re, Pt, Au) could be used to estimate the currently unknown melting curves of Hf and Ir.

PACS numbers: 31.15.A-, 31.15.E-, 64.30.Ef, 64.70.D-

INTRODUCTION

Osmium is a material with exceptional properties. It has the largest mass density (ρ) of all the elemental solids, namely [1, 2] 22.66 g/cc at $(P, T) = (0, 0)$ (iridium is second at 22.65 g/cc) [1], high hardness (second only to chromium among all metals), and extremely low compressibility and thermal expansion. One experimental study indicated that osmium has a bulk modulus, B , higher than that of diamond, the hardest and least compressible of all materials; specifically, at $(P, T) = (0, 300 \text{ K})$, $B \sim 460 \text{ GPa}$ for Os vs. $\sim 440 \text{ GPa}$ for diamond [3]. However, this result was discredited by a subsequent experimental study that obtained $B = 415 \pm 20 \text{ GPa}$ [4]. Its unique properties make Os a potentially important matrix material for the synthesis of superhard materials. Its extremely high bulk modulus and low thermal expansion suggest that Os-based superhard materials may exhibit exceptional mechanical stability under extreme P - T conditions.

The equation of state (EOS) of solid osmium has been extensively studied [5]. Most of the existing data go up to a pressure of 75 GPa [6], and there are isothermal compression data at temperatures up to 3000 K [4], but its melting curve, $T_m(\rho)$ or $T_m(P)$, has never been measured. Even the $P = 0$ melting temperature of Os is uncertain. Very recently, Arblaster [7] found the $P = 0$ melting temperature of pure Os to be $3400 \pm 50 \text{ K}$, which is higher than the value of 3300 K for impure Os that is usually quoted in the literature. A theoretical melting curve to 800 GPa has been constructed on the basis of first-principles calculations of the Grüneisen parameter, $\gamma(\rho)$, and the use of the Lindemann formula for the melting temperature as a function of density, i.e. $d \ln T_m(\rho) / d \ln \rho = 2[\gamma(\rho) - 1/3]$ [8]; melting on the Hugoniot is predicted to occur at $\sim 450 \text{ GPa}$ and $\sim 9200 \text{ K}$. Most recently, Kulyamina *et al.* [9] analyzed all of the isobaric-heating data on Os available in the literature and extracted the initial slope of the Os melting curve: $dT_m(P)/dP = 40.4 \text{ K/GPa}$. We note that their determination is based on the Clausius-Clapeyron relation $dT_m/dP = \Delta V_m / \Delta S_m$, but since neither the volume change at melt, ΔV_m , nor the melting entropy, ΔS_m , are known from experiment, their values can only be estimated. Other, theoretical, values for this slope are 65 K/GPa [10] and 53.4 K/GPa [11].

QMD SIMULATIONS OF EOS AND MELTING CURVE OF OS

Comparison of the $T = 0$ free energies of candidate crystal structures for Os shows that hexagonal close-packed (hcp) is the most stable structure up to at least a compression of two (face-centered cubic, the closest structure to hcp, is ~ 10 mRy/atom higher in energy) [8]. The most recent experimental study [12] reveals that Os retains its hcp structure upon compression to ~ 800 GPa. Hence, we assume that in the pressure range considered in this work Os is a single-phase (hcp) material.

In the present work we determine the melting curve of osmium to ~ 500 GPa using the Z method, which we briefly describe in the following section. Our Z method calculations are carried out using the QMD (quantum molecular dynamics) code VASP (Vienna Ab initio Simulation Package), which is based on density functional theory (DFT). We use the generalized gradient approximation (GGA) with the Perdew-Burke-Ernzerhof (PBE) exchange-correlation functional. We model Os using the electron core-valence representation [$^{48}\text{Cd } 4f^{14} 5p^6 5d^6 6s^2$], i.e. we assign the 14 outermost electrons of Os to the valence. The valence electrons are represented with a plane-wave basis set with a cutoff energy of 400 eV, while the core electrons are represented by projector augmented-wave (PAW) pseudopotentials.

We first calculated the $T = 0$ isotherm of Os. This was done by optimizing the value of c/a , i.e. determining the c/a that minimizes the energy, at a fixed volume of a hexagonal supercell, and then performing a short QMD run and extracting the corresponding value of P . We used a $8 \times 8 \times 5$ (640-atom) supercell with a single Γ -point. With such a large supercell, full energy convergence (to $\lesssim 1$ meV/atom) is already achieved, which was verified by performing short runs with $2 \times 2 \times 2$, $3 \times 3 \times 3$, and $4 \times 4 \times 4$ k -point meshes and comparing their output with that of the 640-atom run with a single Γ -point. We note that, with 14 electrons per atom in the valence, our system has ~ 9000 electrons; to the best of our knowledge, QMD simulations of this magnitude were undertaken only once before: by ourselves in the study on the phase diagram of platinum [13].

In the *ab initio* approach, the density of osmium at $(P, T) = (0, 0)$ is 22.17 g/cc, whereas the experimental value is 22.66 g/cc [1]. Specifically, VASP predicts the lattice constants of the hexagonal unit cell to be (upon optimizing its c/a ratio) $a = 2.7319$ Å and $c = 4.3134$ Å ($c/a = 1.5789$), which corresponds to 22.17 g/cc. The experimental values

are [2] $a = 2.7315 \text{ \AA}$ $c = 4.3148 \text{ \AA}$ ($c/a = 1.5797$), and $\rho = 22.661 \text{ g/cc}$. Alternatively, with VASP, the experimental $(P, T) = (0, 0)$ density of 22.66 g/cc corresponds to $(P, T) = (9.4 \text{ GPa}, 0)$. This 2.2% density mismatch, or 9.4 GPa pressure mismatch, is due to the specific implementation of DFT, namely PBE, in our VASP simulations. In order to directly compare our QMD results to experiment, we will apply the 2.2% density correction (9.4 GPa pressure correction) to all VASP results in the ρ - T (P - T) plane. Specifically, we will multiply VASP densities by 1.022, and subtract 9.4 GPa from VASP pressures. For instance, in Figs. 5 and 6, the system melts at a pressure of 152.8 GPa, while the corresponding melting point is shown in Fig. 7 as having a pressure of 143.4 GPa. Similarly, the same system has a density of 25.41 g/cc, but the corresponding melting point is shown in Fig. 8 as having a density of 25.97 g/cc.

Our results on the $T = 0$ isotherm, as well as the value of c/a as a function of P , are shown in Figs. 1 and 2, respectively. We note that each of the papers [4–6, 14] that discuss Os EOS data uses the third-order Birch-Murnaghan (BM) EOS

$$P(\rho) = \frac{3}{2} B_0 \left(\left(\frac{\rho}{\rho_0} \right)^{7/3} - \left(\frac{\rho}{\rho_0} \right)^{5/3} \right) \left[1 + \frac{3}{4} (B'_0 - 4) \left(\left(\frac{\rho}{\rho_0} \right)^{2/3} - 1 \right) \right],$$

where B_0 and B'_0 are the values of the bulk modulus and its pressure derivative at the reference point $\rho = \rho_0$. Since the $P = 0$ values of the density of Os at $T = 0$ and 300 K differ by $\sim 0.3\%$ (22.66 vs. 22.59 g/cc [1]), and $T = 300 \text{ K}$ introduces a negligibly small thermal pressure correction, the $T = 0$ and $T = 300 \text{ K}$ isotherms can be described by the same values of B_0 and B'_0 . Consequently, we can compare room-temperature isotherm data to our zero-temperature isotherm as determined from QMD. A comparison is shown in Fig. 1. The experimental results from two groups, each of which accessed pressures $P \sim 80 \text{ GPa}$, were presented as BM fits with different choices for B_0 and B'_0 : $B_0 = 421 \text{ GPa}$ and $B'_0 = 4$ from [4], and $B_0 = 395 \text{ GPa}$ and $B'_0 = 5$ from [5]. It is seen that although excellent agreement of the QMD points with the available experimental data (up to $\rho \sim 26 \text{ g/cc}$) is found for either the $B'_0 = 4$ or $B'_0 = 5$ isotherms, it is the third-order Birch-Murnaghan isotherm with $B'_0 = 5$, rather than the more widely accepted $B'_0 = 4$, that best fits the QMD data at densities above the experimental range. We note that for the isotherm data of [14], where $B_0 = 395 \pm 15 \text{ GPa}$ and $B'_0 = 4.5 \pm 0.5$, both values are consistent with [5]. Our fit to the QMD data gives $B_0 = 415.0 \text{ GPa}$ and $B'_0 = 4.87$.

Based on their experimental results on c/a as a function of P , Ocelli *et al.* [6] sug-

gested the existence of an isostructural phase transition in Os at about 25 GPa associated with an anomaly in the compressibility. This anomaly was in turn associated with a discontinuity in the first pressure derivative of the c/a ratio which may arise from the collapse of the “small hole-ellipsoid” [6] in the Fermi surface near the L point. However, subsequent experimental studies did not confirm this c/a anomaly. However, the very recent experiments by Dubrovinsky *et al.* [12] reveal two anomalies, around 150 and 400 GPa, each of which represents a small, $\sim 0.2\%$, reduction in the c/a value. As discussed in [12], the first of these two anomalies may be the signature of a topological change in the Fermi surface for valence electrons, while the second might be related to an electronic transition associated with pressure-induced interactions between core electrons. No such c/a anomalies are seen in our *ab initio* study. In fact, as a function of density, c/a can be fitted with a smooth curve of the form $c/a = \sqrt{8/3} + \alpha/\rho^{5/3} + \beta/\rho^2 + \gamma/\rho^{7/3} + \delta/\rho^{8/3}$ ($\sqrt{8/3}$ is the ideal value of this ratio) over the entire density range; see Fig. 3. As noted in [12], in the case of Os, direct comparison between theory and experiment is not legitimate, because the calculations are carried out at $T = 0$ whereas the experimental data are taken at room temperature. Moreover, for hcp metals, direct comparison between theory and experiment is generally nontrivial: in hcp metals the effect of the electronic transitions on the c/a ratio should become visible at finite T due to the anisotropy of the thermal expansion of the hcp lattice.

Z METHOD CALCULATIONS

To calculate the melting curve of osmium, we used the Z method based on VASP. The Z method was developed to calculate melting curves using first-principles based software, specifically VASP; it was introduced and used for the first time in our paper on the *ab initio* melting curve of Mo [15]. The method has since been applied to the study of a large number of melting curves of different materials [16–18], and comparisons with experimental data on Pb [19], Ta [20], Fe [21], and Pt at ESRF [22] show good agreement. If a material has more than one thermodynamically stable crystal structure, the Z method yields the solid-liquid equilibrium boundaries of those structures. The phase having the highest solid-liquid equilibrium temperature over some pressure range is the most stable, thus the physical melting curve, including triple points, is the envelope of the solid-liquid

equilibrium boundaries. We note that until recently, VASP could only be run for NVE or NVT ensembles, but with the release of the latest version, VASP5.3, we now have the option of running NPT , hence the so-called 2-phase simulations are now an alternative to the Z method.

Fig. 4 shows a typical Z isochore, there comprised of the three green segments AC-CD-DE. It can be approximately mapped out by performing a sequence of QMD runs at progressively higher temperatures and pressures, typically 6-8 points, starting in the solid (segment AB), progressing to the superheated (SH) solid (segment BC), and finally to the liquid (segment DE). If the total energy in a QMD run in the superheated solid is such that the equilibrium temperature $T < T_C$, the final state is on segment AC, but if $T > T_C$ the system melts and the final state is a point (P_l, T_l) on segment DE above the melting curve (dark blue); a further increase in the initial system energy moves the final state up segment DE. Ideally, the QMD runs in the superheated solid would differ by only small temperature increments so that the upper vertex C would be precisely determined, and then a run starting from C would take the system to the point D on the melting curve, but generally this cannot be achieved in practice. The standard implementation of the Z method involves bounding the vertex D from below by the highest calculated state (P_s, T_s) on solid segment AB, and from above by the lowest state (P_l, T_l) on liquid segment DE. Then the melting point can be approximated as $(P_m, T_m) \approx ((P_s + P_l)/2, (T_s + T_l)/2)$. The true melting point must be close to (P_m, T_m) because the actual melting curve crosses the box formed by $P_m \pm (P_l - P_s)/2$ and $T_m \pm (T_l - T_s)/2$.

In contrast to previous melting curve calculations based on the Z method, here the method was utilized as closely as possible to the original concept, but at the expense of an extensive suite of QMD simulations. We calculated eight melting points. At a given density we performed a sequence of very long runs, each up to 25000 time steps or 25 ps, with initial temperatures separated by relatively small increments: 150 K for the first three points on the Os melting curve and 250 K for the remaining five points. We performed 10 such runs for each of the first three points, and 14 runs for each of the remaining five points for a total of 100 runs and ~ 2 million time steps. In the course of these extensive computer simulations, our strategy for detecting the melting point was as follows. The conversion of the initially ordered solid state into a disordered liquid during a QMD run was detected in one of three ways: (i) visual observation of atomic motion in

the computational cell (vibrations around equilibrium sites in a solid vs. diffusion between the sites in a liquid); (ii) a drop in the value of the equilibrium T and the corresponding jump in the value of the equilibrium P ; (iii) change in the radial distribution function (a long sequence of well-pronounced peaks in a solid vs. a few peaks in a liquid). If the system did not melt during the 25 ps of running time, we started the next run with an initial T higher by 150-250 K than the previous one, *etc.* The first run in which the system melts during the 25 ps of running time was assumed to correspond to the upper vertex C; during this run the complete melting process corresponding to the C \rightarrow D transition in Fig. 4 is usually observed. We refer to such a run as the melting run. With an even higher initial T , the system melts at an earlier time than in the melting run, and the duration of the melting process shortens; both the time when melting begins and the duration of the process decrease with increasing T , and for a sufficiently high initial T the system melts immediately.

In Figs. 5 and 6 we illustrate the temperature and pressure evolution of runs with initial temperatures of 21000, 21250, and 21500 K; these runs correspond to the Os melting point at ~ 145 GPa in Fig. 7. In the 21000 K run, the system remains a superheated solid. In the 21250 K run, the system starts melting at about 9 ps, and the melting process takes approximately 3 ps. With an additional 250 K increase in the initial T , melting begins at ~ 4 ps and the process takes 2-2.5 ps.

We now estimate the uncertainty in the melting temperature for the computational procedure outlined above.

First of all, changes in P are typically much smaller than that in T . For instance, as seen in Figs. 5 and 6, which typify T and P changes during simulated melting, the pressure changes by less than 10% while $\Delta T \sim 25\%$. We estimate the errors in P to range from a few GPa at low pressures to ~ 10 GPa at the highest pressure considered; such errors do not exceed the size of the points in Fig. 7. As a reasonable approximation, we can ignore errors in P .

The error in the melting temperature is due to the uncertainty in the maximum temperature for which the Os remains a superheated solid, i.e. the temperature at vertex C in Fig. 4. Assume that the melting occurs from a superheated solid state C' which lies on the continuation of segment BC in Fig. 4 beyond point C; the temperature at C is T_{SH} and that at C' is $T_{SH} + \Delta T_{SH}$. Melting from C takes the system to point D at temperature T_m ,

while melting from C' leaves the system in a liquid state D' on segment DE at temperature $T_m + \Delta T_m$. Following [23], we now consider energy balance for the virtual transitions $B \rightarrow C$ and $B \rightarrow D_{liq}$. The energy increase for $B \rightarrow C$ is $C_{VS} (T_{SH} - T_m^{(B)})$, where C_{VS} is the solid heat capacity at constant volume and $T_m^{(B)}$ is the melting temperature at B. The transition $B \rightarrow D_{liq}$ can be decomposed into $B \rightarrow D_{sol}$ with energy change $C_{VS} (T_m - T_m^{(B)})$, and then melting at D with an energy increase of $T_m \Delta S_m$, where ΔS_m is the entropy of melting; thus the total energy change for $B \rightarrow D_{liq}$ is $C_{VS} (T_m - T_m^{(B)}) + T_m \Delta S_m$. Since points C and D_{liq} have the same energy, we can equate the energy changes for $B \rightarrow C$ and $B \rightarrow D_{liq}$ ($T_m^{(B)}$ drops out):

$$C_{VS} (T_{SH} - T_m) = T_m \Delta S_m. \quad (1)$$

Similarly, for $B \rightarrow C'$ and $B \rightarrow D'$ we have

$$C_{VS} (T_{SH} + \Delta T_{SH} - T_m) = T_m \Delta S_m + C_{VL} \Delta T_m. \quad (2)$$

Here C_{VL} is the liquid heat capacity at constant volume. It then follows from (1) and (2) that

$$\Delta T_m = \frac{C_{VS}}{C_{VL}} \Delta T_{SH}. \quad (3)$$

In the vicinity of the melting point the solid and liquid heat capacities are known to be approximately equal [24], hence

$$\Delta T_m \approx \Delta T_{SH}. \quad (4)$$

We have the simple result that the error in T_m is approximately equal to the difference in the temperatures for the first run during which melting occurs and the true melting run.

The temperature difference between two solid states on segment AC in Fig. 4 is about half of the difference of the initial temperatures in the QMD runs. This is so because during a QMD run the initial thermal energy, which is the total system energy, is divided almost equally into potential and kinetic energies, and the latter is the thermal energy of the final state. Therefore, ΔT_{SH} cannot exceed one half of the difference of the initial temperatures for the first run during which the system melts and the last run during which the system remains superheated. For the present Os calculations, this implies a maximum error of ~ 75 K for the first three points on the *ab initio* melting curve and ~ 125 K for the remaining five points.

ZERO PRESSURE MELTING TEMPERATURE AND DENSITY

The zero pressure melting temperature of Os was recently found by Arblaster to be 3400 ± 50 K [7]. However, by making use of our new QMD melting temperatures and experimental results on the $P = 0$ thermal expansion of Os, which span temperatures from 0 to 2200 K [25] and 1300 K [26], we can provide a more reliable value for the $P = 0$ melting temperature of Os.

We first take the three lowest- P QMD melting points and fit them with a polynomial in the ρ - T plane. We then extrapolate the $P = 0$ thermal expansion data of refs. [25, 26] using a polynomial fit. The point of intersection of both fits determines the ρ - T coordinates of the $P = 0$ melting point; we find $T_m(P = 0) = 3370$ K and $\rho_m(P = 0) = 20.4$ g/cc. We note that different fits to the first few QMD points in the P - T plane (a polynomial fit, or a fit of the form $T_m(P) = T_{m1} + a(P - P_1)^b$ where (P_1, T_{m1}) are the P - T coordinates of the first point, etc.) give values of $T_m(P = 0)$ in the range 3360-3369 K, depending on the number of points used, consistent with the above 3370 K. We therefore take 3370 K to be the central value of the $P = 0$ melting temperature of osmium. Hence, our *ab initio* results confirm Arblaster's conclusion [7] that 3400 ± 50 K is a better estimate for $T_m(P = 0)$ than the value 3300 K quoted in the current literature. Upon taking into account a possible error of 75 K (see the previous section) our *ab initio* $P = 0$ melting point of Os is

$$T_m(P = 0) = 3370 \pm 75 \text{ K.} \quad (5)$$

THE *AB INITIO* MELTING CURVE OF OS

An analytic expression for the melting curve of Os in the P - T plane can be constructed as the best fit of the Simon form, $T_m(P) = T_m(0)(1 + P/a)^b$, to all eight QMD points with $T_m(0) = 3370$ K. The result is (T in K, P in GPa)

$$T_m(P) = 3370 \left(1 + \frac{P}{36.065}\right)^{0.530}. \quad (6)$$

For Eqs. (5) and (6), $dT_m(P)/dP = (49.5 \pm 1.1)$ K/GPa at $P = 0$, in good agreement with the values from [9–11]. The melting curve (6) is shown in Fig. 7 along with the eight QMD melting points. The maximum errors quoted in the previous section, viz. ~ 75 K for the

first three points and ~ 125 K for the remaining five points, lie within the corresponding symbols in the figure.

We now consider the melting curve of Os in ρ - T coordinates; $T_m(\rho)$ is useful for a number of engineering applications (e.g., constitutive modeling). Following [27, 28], the ρ - T melting curve is described by the Lindemann relation, $d \ln T_m(\rho)/d \ln \rho = 2 [\gamma(\rho) - 1/3]$, with a Grüneisen parameter of the form $\gamma(\rho) = 1/2 + \gamma_1/\rho^{1/3} + \gamma_2/\rho^q$. The three parameters γ_1 , γ_2 and q are determined by imposing three conditions. One of the conditions, the equality of the $\rho \rightarrow \infty$ limit of the melting curve as described by the above Grüneisen parameter and the one-component plasma (OCP) limit, reduces to the equation [27, 28]

$$T_m v_m^{1/3} \exp \left\{ \frac{6\gamma_1}{\rho_m^{1/3}} + \frac{2\gamma_2}{q \rho_m^q} \right\} = \left(\frac{4\pi}{3} \right)^{1/3} \frac{e^2}{k_B} \frac{Z^2}{\Gamma_m},$$

where T_m , ρ_m , and v_m are the $P = 0$ melting point, density at melt, and unit cell volume at melt, respectively (see previous section), and $\Gamma_m = 175$ is the OCP coupling parameter at melt [27, 28]. As our second condition we equate γ at $\rho(T = 0, P = 0) = 22.66$ g/cc to the experimental value of 2.0 [29]. Ideally, the third condition is the equality of $\gamma(\rho_m) = 1/2 + \gamma_1/\rho_m^{1/3} + \gamma_2/\rho_m^q$ and its value as given in terms of the initial slope of the melting curve in ρ - T space (which follows from the above Lindemann relation):

$$\gamma(\rho_m) = \frac{1}{2} \frac{\rho_m}{T_m} \frac{dT_m}{d\rho_m} + \frac{1}{3}. \quad (7)$$

The melting curve of Os has never been measured, and so the value of $\gamma(\rho_m)$ is not available from experiment. We could extract it from our *ab initio* ρ - T melting curve, which would ensure that the resulting (γ_1, γ_2, q) melting curve agrees with the QMD data, but instead we obtain the set of three parameters independently of QMD as a consistency check between QMD and the (γ_1, γ_2, q) theoretical scheme. In lieu of using (7) to obtain $\gamma(\rho_m)$, our third condition is the assumption that the value of γ_1 satisfies the $\gamma_1 = \gamma_1(Z)$ systematics established in [27, 28]. Specifically, the formula for γ_1 as a function of Z predicts that for Os ($Z = 76$), $\gamma_1 = 3.0 - 3.12$; we take $\gamma_1 = 3.06$. With $\gamma(22.66 \text{ g/cc})=2.0$, the values of γ_2 and q are easily found by solving the first two conditions. In this way we determine that the values of the three parameters are

$$\gamma_1 = 3.06, \quad \gamma_2 = 4.1 \cdot 10^{15}, \quad q = 11.8, \quad (8)$$

where the units of γ_1 and γ_2 are $(\text{g/cc})^{1/3}$ and $(\text{g/cc})^q$, respectively. The ρ - T melting curve of Os with the above set of parameters is shown in Fig. 8. As clearly seen, this

curve is in excellent agreement with the eight QMD points also shown in Fig. 8. However, the ρ - T melting curve of Joshi *et al.* [8] (dashed line in Fig. 8), which we calculated using their Grüneisen parameter and the Lindemann formula, disagrees with our *ab initio* ρ - T melting data. Also, its P - T counterpart disagrees with our *ab initio* P - T melting curve in Fig. 7. In particular, at the Hugoniot melting point at 450 GPa, our melting curve gives $T_m(450 \text{ GPa}) \sim 13400 \text{ K}$ while Joshi *et al.* find $T_m(450 \text{ GPa}) \sim 9200 \text{ K}$.

Although the results of Joshi *et al.* and ours are both based on first principles, the density dependences of the Grüneisen parameters differ significantly. Since there is a density mismatch of a similar magnitude to ours (3.15% vs. 2.2%) in the *ab initio* approach of Joshi *et al.* [8], we first adjust their Grüneisen parameter accordingly in order to make a direct comparison with ours, which is based on experimental data. Both Grüneisen parameters are shown in Fig. 9. It is seen that their difference does not exceed $\sim 5\%$. The most probable reason for the discrepancy between the melting curve of Joshi *et al.* and our QMD data is their unphysical choice for the density dependence of the Grüneisen parameter, viz. $\gamma(\eta) = a + b\eta + c\eta^2 + d\eta^3$ where $\eta \equiv \rho_0/\rho$, and $a \neq 1/2$; it follows from the theory of the OCP that $a \rightarrow 1/2$ as $\rho \rightarrow \infty$ [27, 28]. Their choice for the density dependence of the Grüneisen parameter results in the unphysical melting curve.

MELTING CURVES OF THE 3RD-ROW TRANSITION METALS

Of all the 3rd-row transition metals, only the melting curves of Hf and Ir have never been measured or calculated. In addition to the melting curve of Os calculated in this work, in Fig. 10 we also plot the melting curves of Ta [16, 20], W [30], Re [31], Pt [13, 18, 22], and Au [32–34]. As seen in Fig. 10, all six melting curves have low curvature and comparable slopes, roughly 50 K/GPa. These regularities plus approximate $P = 0$ melting temperatures could be used to estimate the currently unknown melting curves of Hf and Ir.

CONCLUDING REMARKS

We have obtained the melting curve of Os using the Z method based on first-principles QMD. We have run a total of about 2 million time steps in our QMD simulations; however,

the high accuracy of the results and their importance to the field of phase diagram studies justifies the computational cost. The *ab initio* zero-pressure melting point of Os is 3370 ± 75 K; this range encompasses all of the available data in the literature and corroborates the conclusion of Arblaster. We have identified a possible reason for the disagreement between our QMD results and the melting curve of Os obtained by Joshi *et al.* that is also based on first principles. Regularities in the melting curves of Os and five other 3rd-row transition metals could be used to estimate the currently unknown melting curves of Hf and Ir.

ACKNOWLEDGMENTS

The work was done under the auspices of the US DOE/NNSA. The QMD calculations were performed on the LANL clusters Conejo and Mapache.

REFERENCES

-
- [1] J.W. Arblaster, Johnson Matthey Technol. Rev. **58**, 137 (2014)
 - [2] J.W. Arblaster, Platinum Metals Rev. **57**, 177 (2013)
 - [3] H. Cynn, J.E. Klepeis, C.-S. Yoo, and D.A. Young, Phys. Rev. Lett. **88**, 135701 (2002)
 - [4] M.M. Armentrout and A. Kavner, J. Appl. Phys. **107**, 093528 (2010) and references therein
 - [5] B.K. Godwal, J. Yan, S.M. Clark, and R. Jeanloz, J. Appl. Phys. **111**, 112608 (2012) and references therein
 - [6] F. Occelli, D.L. Farber, J. Badro, C.M. Aracne, D.M. Teter, M. Hanfland, B. Canny, and B. Couzinet, Phys. Rev. Lett. **93**, 095502 (2004)
 - [7] J.W. Arblaster, Platinum Metals Rev. **49**, 166 (2005) and references therein
 - [8] K.D. Joshi, S.C. Gupta, and S. Banerjee, J. Phys. Cond. Matt. **21**, 415402 (2009)
 - [9] E.Yu. Kulyamina, V.Yu. Zitserman, and L.R. Fokin, High Temperature **53**, 151 (2015)
 - [10] A.R. Regel' and V.M. Glazov, V.M., *Periodicheskiy zakon i fizicheskie svoistva elektronnykh rasplavov* (The Periodic Law and Physical Properties of Electronic Melts) (Nauka, Moscow, 1978)

- [11] T. Gorecki, Z. Metallk. **68**, 231 (1977); High Temp. - High Pres. **11**, 683 (1979)
- [12] L. Dubrovinsky, N. Dubrovinskaya, E. Bykova, M. Bykov, V. Prakapenka, C. Prescher, K. Glazyrin, H.-P. Liermann, M. Hanfland, M. Ekholm, G. Feng, L.V. Pourovskii, M.I. Katsnelson, J.M. Wills, and I.A. Abrikosov, Nature **525**, 226 (2015)
- [13] L. Burakovsky, S.P. Chen, D.L. Preston, and D.G. Sheppard, J. Phys. Conf. Ser. **500**, 162001 (2014)
- [14] T. Kenichi, Phys. Rev. B **70**, 012101 (2004)
- [15] A.B. Belonoshko, L. Burakovsky, S.P. Chen, B. Johansson, A.S. Mikhaylushkin, D.L. Preston, S.I. Simak, and D.C. Swift, Phys. Rev. Lett. **100**, 135701 (2008)
- [16] L. Burakovsky, S.P. Chen, D.L. Preston, A.B. Belonoshko, A. Rosengren, A.S. Mikhaylushkin, S.I. Simak, and J.A. Moriarty, Phys. Rev. Lett. **104**, 255702 (2010) and references therein
- [17] A.B. Belonoshko, A. Rosengren, L. Burakovsky, D.L. Preston, and B. Johansson, Phys. Rev. B **79**, 220102(R) (2009)
- [18] A.B. Belonoshko and A. Rosengren, Phys. Rev. B **85**, 174104 (2012) and references therein
- [19] A. Dewaele, M. Mezouar, N. Guignot and P. Loubeyre, Phys. Rev. B **76**, 144106 (2007)
- [20] A. Dewaele, M. Mezouar, N. Guignot and P. Loubeyre, Phys. Rev. Lett. **104**, 255701 (2010)
- [21] S. Anzellini, A. Dewaele, M. Mezouar, P. Loubeyre, and G. Morard, Science **340**, 464 (2013)
- [22] D. Errandonea, Phys. Rev. B **87**, 054108 (2013)
- [23] A.B. Belonoshko, N.V. Skorodumova, A. Rosengren and B. Johansson, Phys. Rev. B **73**, 012201 (2006)
- [24] R. Grover, J. Chem. Phys. **55**, 3435 (1971); “Metallic high pressure equation of state derived from experimental data,” in *High Pressure Science and Technology, Proceedings of the 6th AIRAPT Conference*, (Plenum Press, N.Y., 1979), Vol. 1, p. 33. It is suggested in the second paper that, for C_{VL} at a given density, $C_{VL} = \frac{3}{2} R \left[1 + (1 + 0.1 T/T_m)^{-1} \right]$ is a good average representation of all the available experimental data and computer simulations on liquid metals, including those for the OCP. Hence, at $T = T_m$, $C_{VL} = \frac{63}{22} R$. Since $C_{VS} \cong 3R$, $C_{VL} \cong \frac{21}{22} C_{VS} \approx C_{VS}$.
- [25] V.E. Zinov'ev, *Handbook of Thermophysical Properties of Metals at High Temperatures*, (Nova Science Publishers, New York, 1996), p. 328
- [26] J.W. Arblaster, Platinum Metals Rev. **57**, 177 (2013)

- [27] L. Burakovsky and D.L. Preston, *J. Phys. Chem. Sol.* **65**, 1581 (2004) and references therein
- [28] L. Burakovsky and D.L. Preston, *Recent Res. Devel. Physics* **5**, 193 (2004) and references therein
- [29] The value in the text, i.e. 2.0, comes from averaging the following values available in the literature: 2.02 from K. Gschneidner, *Solid State Physics* (Academic Press, New York and London, 1964), Vol. 16, p. 275; 1.77 ± 0.12 from Yu.S. Ponosov *et al.*, *Phys. Rev. B* **71**, 220301(R) (2005); 2.12 from C. Pantea *et al.*, *Phys. Rev. B* **80**, 024112 (2009)
- [30] C.-M. Liu, X.-R. Chen, C. Xu, L.-C. Cai, and F.-Q. Jing, *J. Appl. Phys.* **112**, 013518 (2012)
- [31] L.F. Vereshchagin, N.S. Fateeva, and M.V. Magnitskaya, *JETP Lett.* **22**, 106 (1975)
- [32] D.L. Decker and H.B. Vanfleet, *Phys. Rev.* **138**, A129 (1965)
- [33] T. Tsuchiya, *J. Geophys. Res.* **108**, 2462 (2003)
- [34] T. Pippinger, L. Dubrovinsky, K. Glazyrin, R. Miletich, and N. Dubrovinskaya, *Fisica de la Tierra* **23**, 29 (2011)

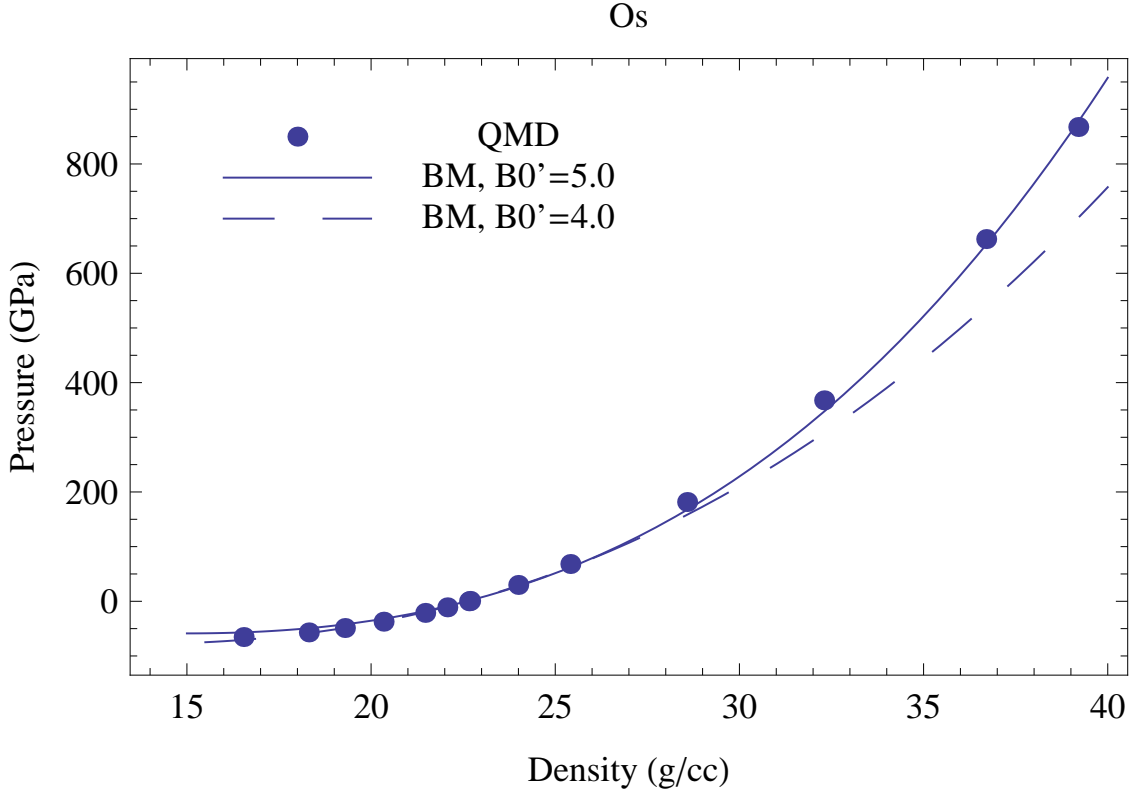


FIG. 1: The $T = 0$ Os EOS from VASP compared to the experimental 300 K Birch-Murnagan (BM) EOSs with $B'_0 = 4.0$ and 5.0 . In the experimental pressure range of $0 - 80$ GPa ($22.6 \leq \rho \lesssim 26$ g/cc) both EOSs virtually coincide.

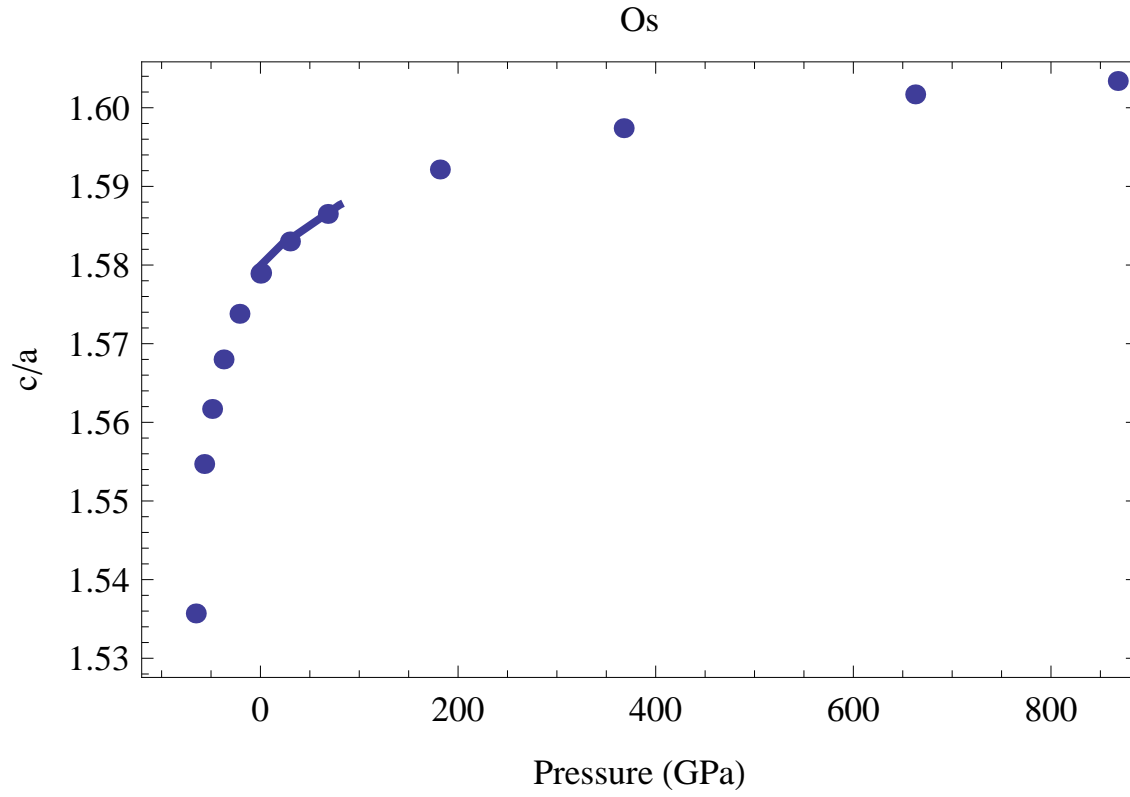


FIG. 2: The c/a ratio as a function of P . The available experimental data are indicated with thick line from [6].

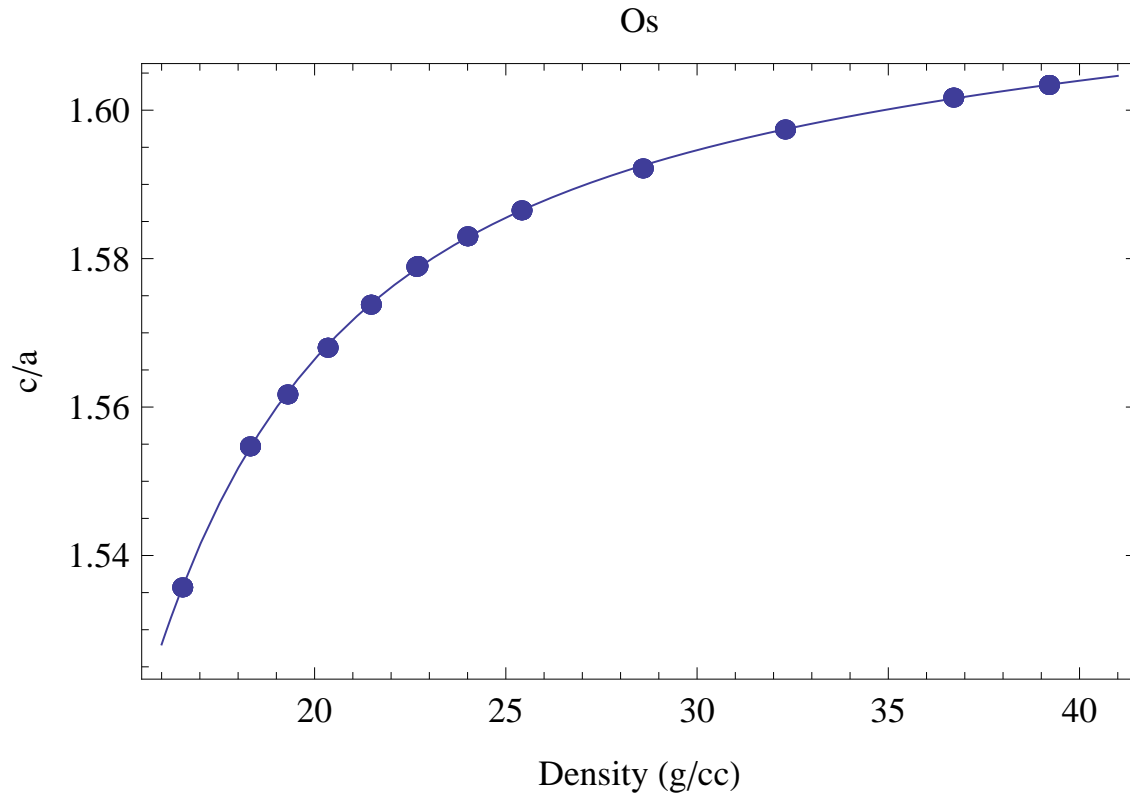


FIG. 3: The c/a ratio as a function of density, along with the corresponding fitting curve.

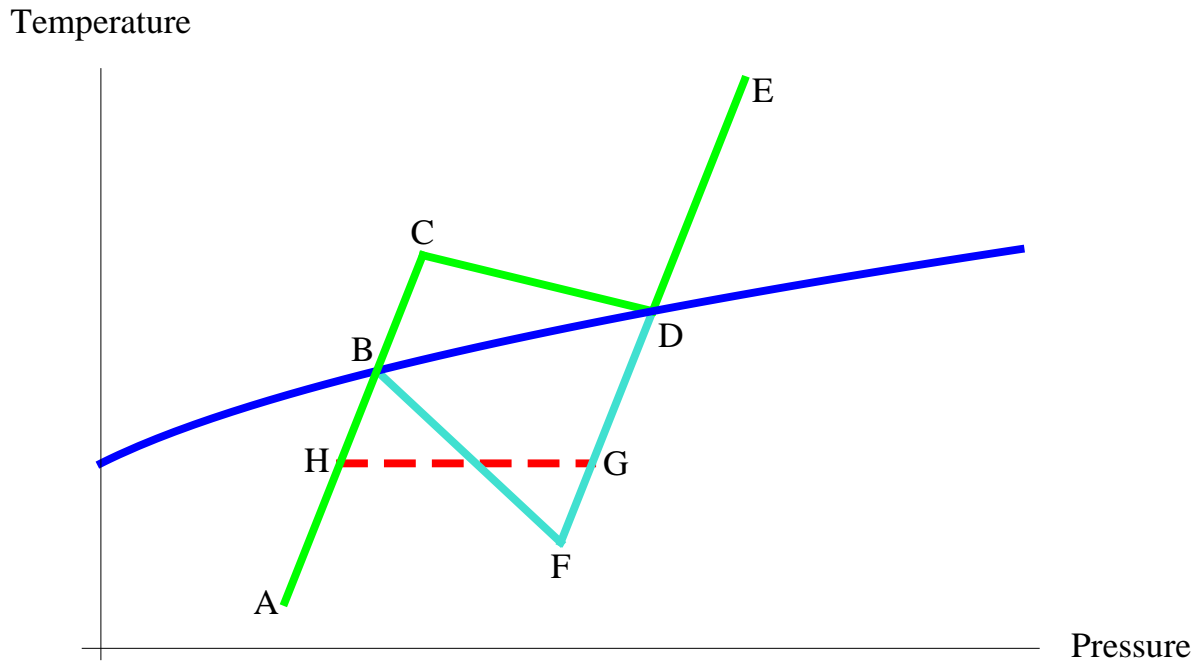


FIG. 4: Typical isochore used in the Z methodology. Different segments of the isochore correspond to solid (AB), superheated solid (BC), liquid (DE), and supercooled liquid (DF) states. Melting corresponds to segment CD. Isochoric and isothermal solidification processes correspond to segments FB and GH, respectively, and are used in the so-called inverse Z method [13].

Os, $a = 2.6 \text{ \AA}$

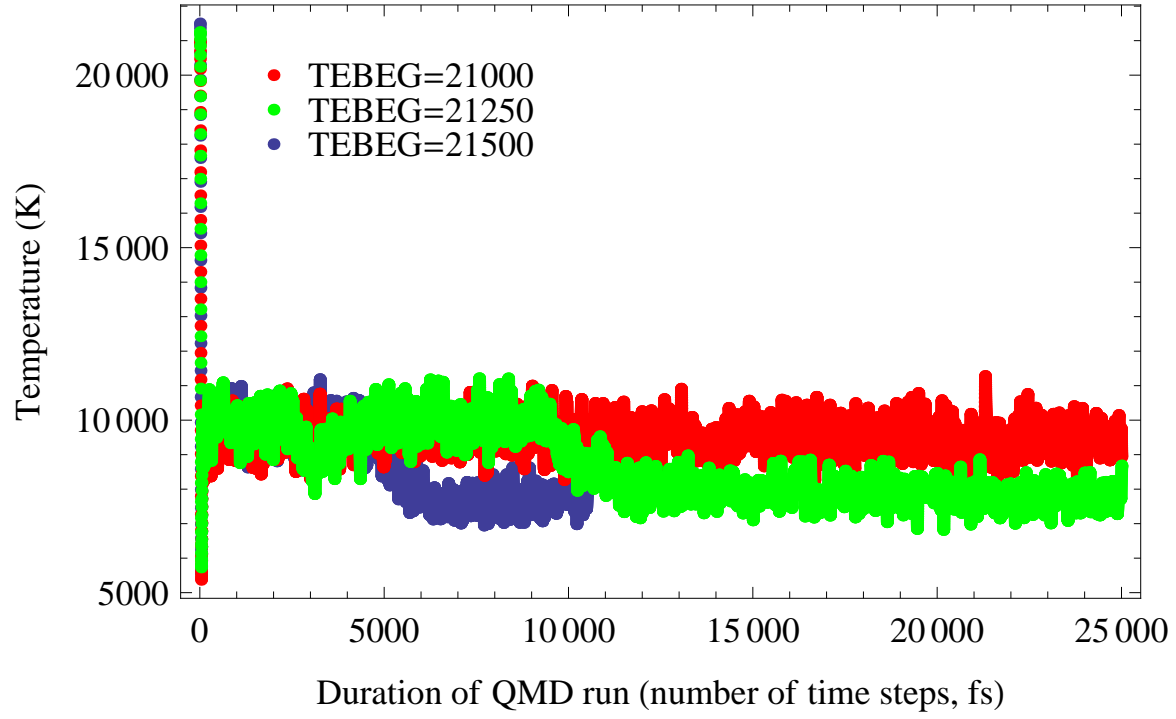


FIG. 5: Time evolution of temperature in three QMD runs with initial temperatures (TEBEGs) separated by 250 K. The middle run is the melting run, during which T decreases from ~ 10000 K for the superheated state to ~ 8000 K for the liquid at the corresponding melting point.

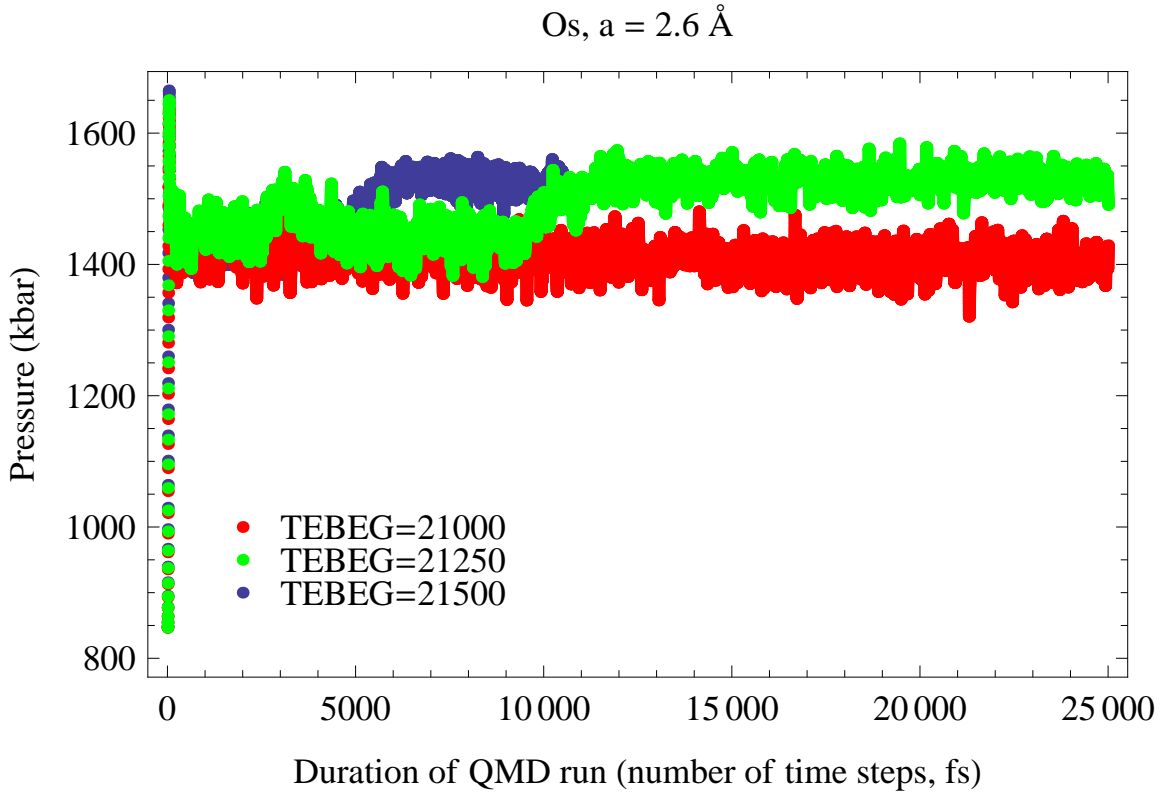


FIG. 6: The same as in Fig. 5 for the time evolution of pressure. During melting P increases from ~ 140 GPa for the superheated state to ~ 153 GPa for the liquid at the corresponding melting point.

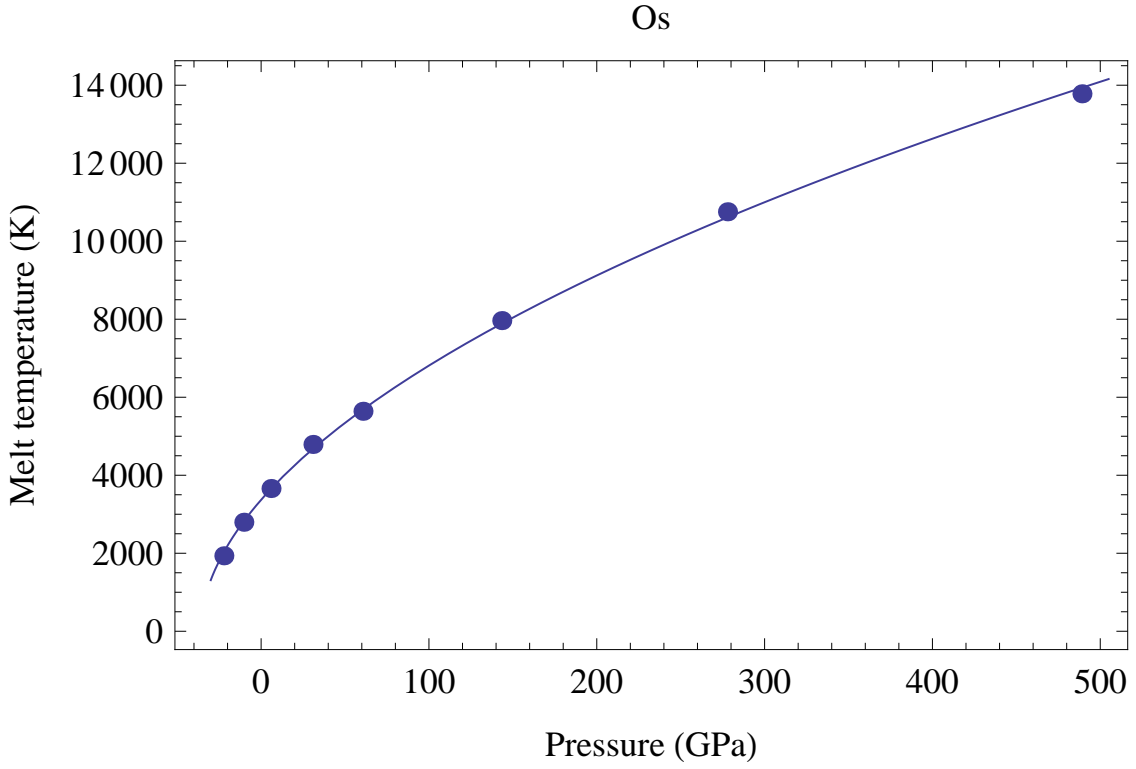


FIG. 7: The QMD-based melting curve of Os in P - T coordinates: VASP results (bullets) and the corresponding Simon equation, Eq. (5).

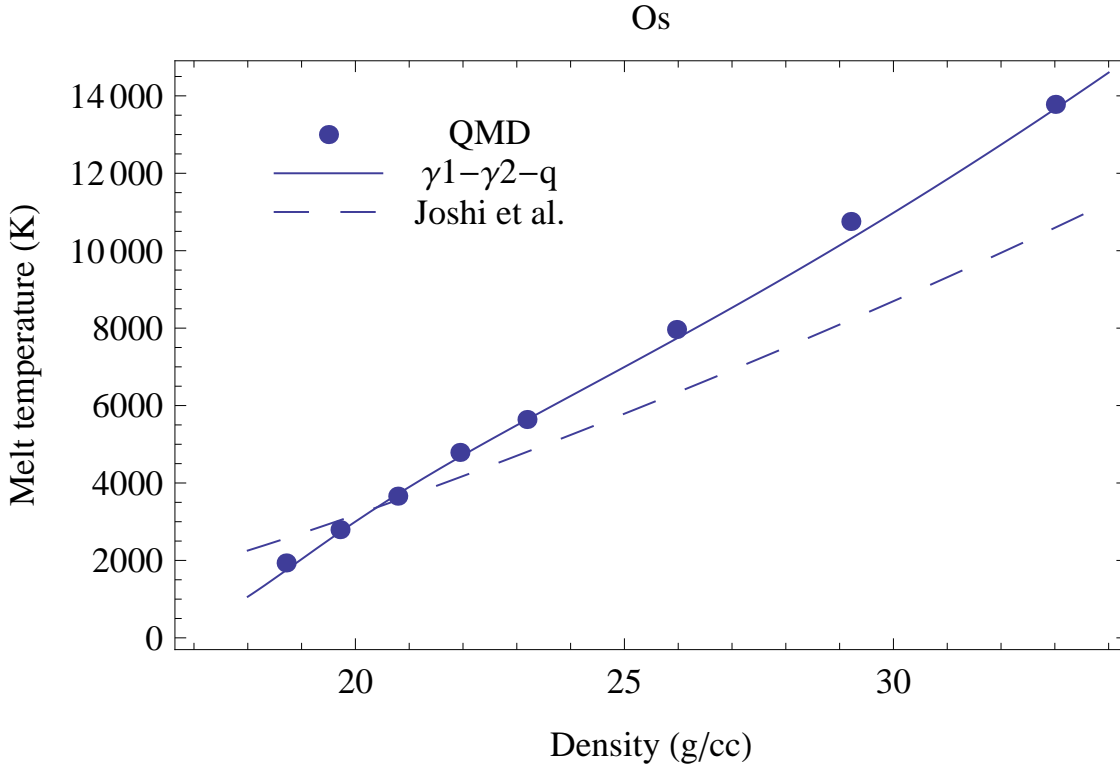


FIG. 8: The QMD-based melting curve of Os in density-temperature coordinates vs. the two theoretical formulations described in the text.

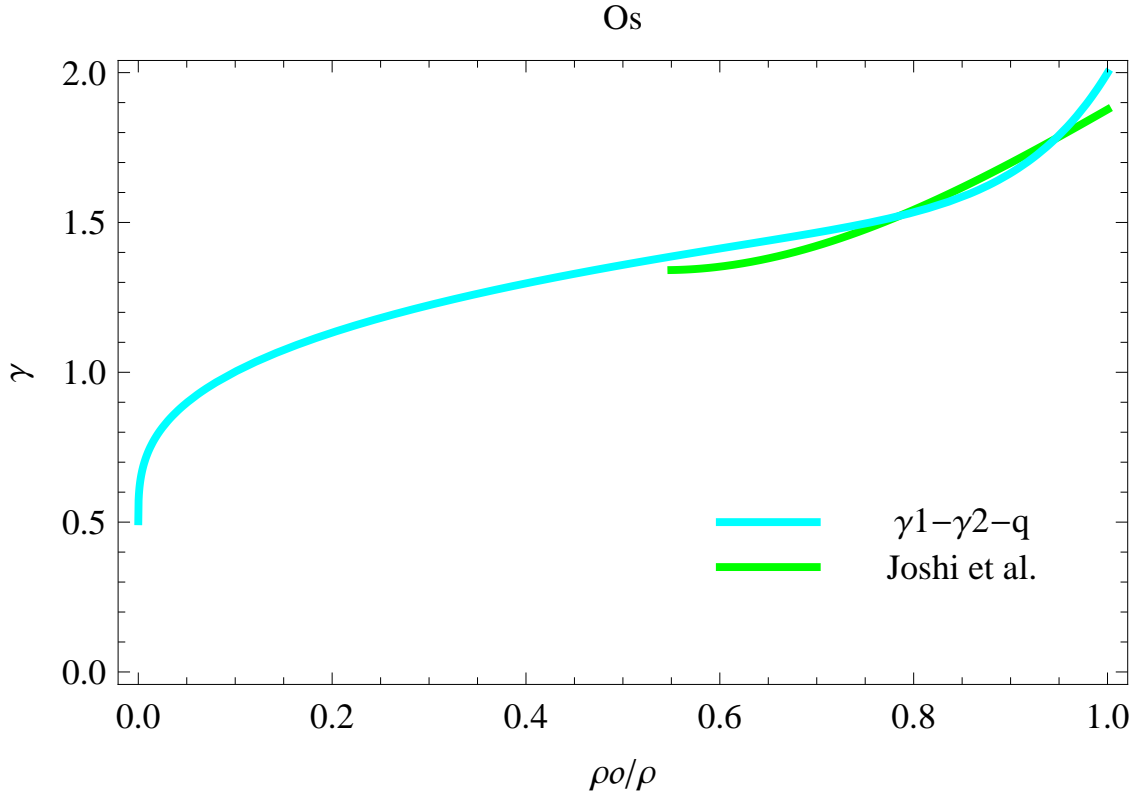


FIG. 9: Comparison of the density dependences of the Grüneisen parameters in the two theoretical formulations described in the text.

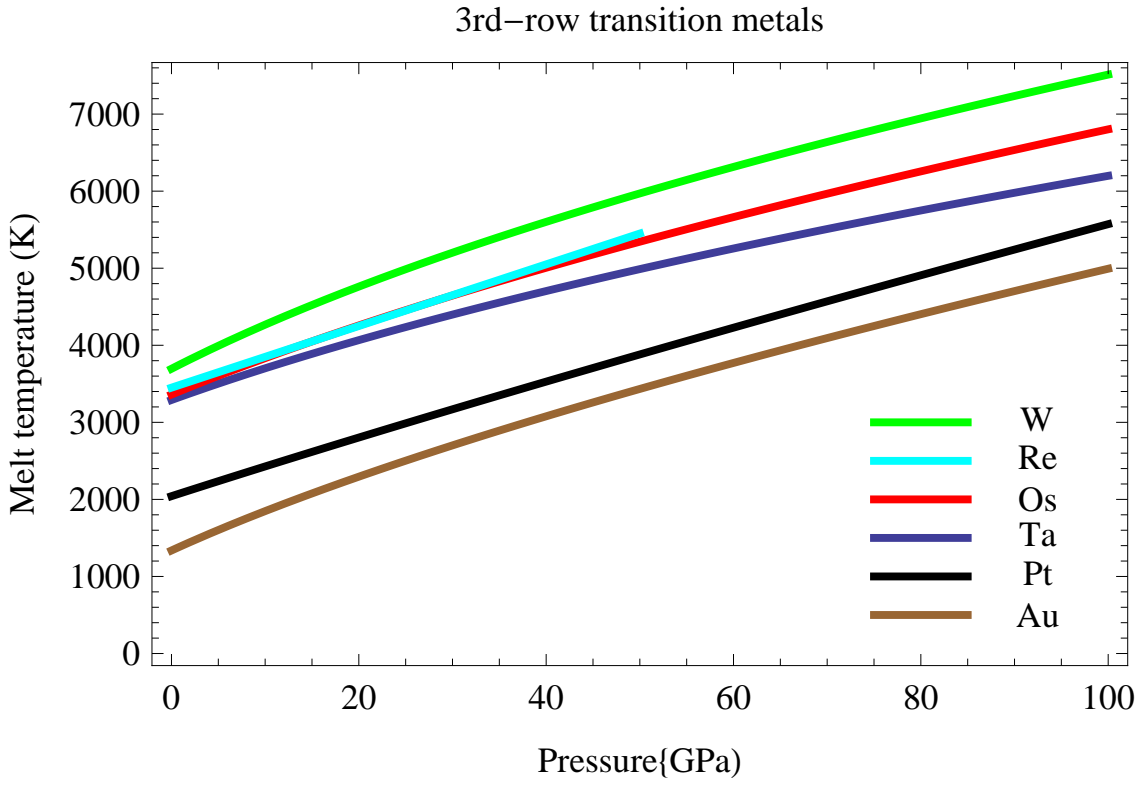


FIG. 10: The melting systematics of the 3rd-row transition metals based on the available experimental and/or theoretical data.